Multi-parameter photon-by-photon hidden Markov modeling

Paul David Harris*[1], Alessandra Narducci[2], Christian Gebhardt[2], Thorben Cordes[2], Shimon Weiss[3,4], and Eitan Lerner†[1,5]

[1]Department of Biological Chemistry, The Alexander Silberman Institute of Life Sciences, Faculty of Mathematics & Science, The Edmond J. Safra Campus, The Hebrew University of Jerusalem, Jerusalem 9190401, Israel
[2]Physical and Synthetic Biology. Faculty of Biology, Ludwig-Maximilians-Universität München, Großhadernerstr. 2-4, 82152 Planegg-Martinsried, Germany
[3]Department of Chemistry and Biochemistry, and Department of Physiology, University of California, Los Angeles, California, United States
[4]Department of Physiology, CaliforniaNanoSystems Institute, University of California, Los Angeles, California, United States
[5]The Center for Nanoscience and Nanotechnology, The Hebrew University of Jerusalem, Jerusalem 9190401, Israel

October 13, 2021

Abstract

Single-molecule Förster resonance energy transfer (smFRET) is a unique biophysical approach for studying conformational dynamics in biomacromolecules. Photon-by-photon hidden Markov modelling (H^2MM) is an analysis tool that can quantify FRET dynamics of single biomolecules, even if they occur on the sub-millisecond timescale. However, dye photophysical transitions intertwined with FRET dynamics may introduce artefacts. Here, we introduce multi-parameter H^2MM (mpH^2MM), which assists in identifying FRET dynamics based on simultaneous observation of multiple experimentally-derived parameters. We show the importance of using mpH^2MM to decouple FRET dynamics caused by conformational

*paul.harris@mail.huji.ac.il
†eitan.lerner@mail.huji.ac.il

changes from photophysical transitions in confocal-based smFRET measurements of a DNA hairpin, the maltose binding protein, MalE, and the type-III secretion system effector, YopO, from *Yersinia* species all exhibiting conformational dynamics ranging from the sub-second to microsecond timescales. Overall, we show that using mpH^{2}MM facilitates the identification and quantification of biomolecular sub-populations and their origin.

1 Introduction

The role of structural dynamics in biomolecular function has come to the forefront of biophysical research[1, 2]. Biomolecules in solution exhibit structural dynamics at a hierarchy of timescales and modes, from bond rotations to movements of entire globular domains, occurring at times from picoseconds to seconds and longer[3]. In many cases, the stages in the biomolecular function are promoted by different sub-populations of closely-related structures, or conformations. Examples include coupling of catalytic activity to domain dynamics in some enzymes[4, 5], the dynamics of the DNA bubble in transcription initiation to support transcription start site selection[6, 7], DNA mismatch repair[8], protein translocation[9], chaperone action[10], the allosteric regulation of the AAA+ disaggregase[11], active membrane transport[12–17], and many other important biochemical processes, in which structural dynamics is coupled to or influences biological function[1, 2]. Thus, methods capable of identifying and characterizing distinctly time-separated structural sub-populations of biomolecules are of great interest in biomolecular sciences and structural biology.

NMR- and EPR-based methods[18–21] as well as single-molecule methods[22–26] have come to the forefront in the field of dynamic structural biology, each with their own advantages and limitations. Single-molecule methods allow probing one biomolecule at a time while tracking multiple experimental parameters simultaneously. This approach provides access to conformational heterogeneity, real-time kinetics and identification of rare conformational states otherwise masked due to ensemble averaging.

One of the most popular single-molecule approaches relies on the phenomenon of Förster resonance energy transfer (FRET), single-molecule FRET (smFRET)[27], where the biomolecule of interest is site-specifically labeled at two strategic residues with two fluorescent dyes, which can exhibit transfer of excitation energy from the donor dye to the acceptor dye with a probability (or efficiency; E), which is inversely proportional to the sixth power of the distance between the dyes, according to the Förster relation[28–30]. The FRET efficiency can be determined either ratiometrically, through the donor and acceptor fluorescence intensities, or through the use of fluorescence lifetime-based methods. Ratiometric methods yield an initial raw efficiency, E_{raw} (see supplementary equation S1), to which correction factors must be applied, such as leakage of donor photons into the acceptor channel, direct excitation of the acceptor by the donor

light source, differences in donor and acceptor fluorescence quantum yields and detection efficiencies (better known as the γ-factor), in order to yield accurate E[31–33]. Lifetime-based approaches do not require such corrections, but rely on pulsed laser sources and time-correlated single-photon counting modules[34]. SmFRET has proven to be a powerful tool to disentangle conformational sub-populations of bio-macromolecules undergoing dynamic transitions over a range of timescales[3]. Nevertheless, smFRET remains limited by the time resolution and observation time of the apparatus[3]. A popular approach is the observation of individual freely-diffusing molecules through the excitation volume of a confocal microscope[1, 2]. Here the observation time of a single molecule is on the order of a few milliseconds, with possible time-resolution of dynamics as rapid as nanoseconds using advanced analyses of photon statistics within single-molecule photon bursts (figure 1a,b). Some of the latter methods include photon distribution analysis, or probability distribution analysis (PDA)[35–40], burst variance analysis (BVA)[41], FRET two-kernel density estimator (FRET-2CDE)[42], analysis of two-dimensional histograms of donor fluorescence lifetimes and ratiometric FRET efficiencies of bursts, also known as FRET lines[34, 43, 44], fluorescence correlation spectroscopy (FCS)[45, 46] coupled to FRET[47–49], maximum likelihood approaches[50–54], such as hidden Markov modeling[4, 7, 55, 56] (HMM) and photon recoloring[57, 58]. These have been summarized in recent reviews of the field[1, 2].

Photon-by-photon hidden Markov modelling (H^2MM)[56] is a maximum likelihood method[57, 59] that adopts the HMM machinery, while working directly with the photon data without prior binning into fluorescence intensity time traces. H^2MM can extract the number of states involved in the underlying FRET dynamics, their mean E_{raw} values and transition rate constants. Nevertheless, while advanced smFRET setups often detect multiple fluorescence parameters beyond the intensities, such as in alternating-laser excitation (ALEX)[60, 61] or in multi-color smFRET-based measurements[62–69], H^2MM in its current iteration only uses the raw FRET efficiency of a single donor-acceptor pair of dyes.

Here, we introduce multi-parameter H^2MM (mpH^2MM), which enables incorporation of multiple parameters in the analysis, through additional photon streams. We demonstrate this concept with two types of ALEX experiments: microsecond ALEX (µsALEX) and nanosecond ALEX (nsALEX; known also as pulsed interleaved excitation, PIE)[60, 61]. We applied this approach to different biomacromolecular complexes with dynamics ranging from the sub-second to microsecond timescales: (i) a DNA hairpin loop[70], (ii) the maltose binding protein MalE from *E. coli*, and (iii) YopO, a type-III-secretion system effector from pathogenic *Yersinia* species[71] (figure 1c-e, figure S1). Our results and analysis demonstrate that mpH^2MM is able to quantitatively report sub-populations based on both the ALEX-relevant mean parameters, E_{raw} and the stoichiometry, S_{raw} (see supplementary equation S2), as well as their transition rate constants, demonstrating FRET-relevant conformational transitions, as well as FRET-irrelevant photophysical transitions. We also present the H2MM_C python package[72], with a backend written in C, for data process-

ing, which is approximately two orders of magnitude faster than the previous implementation of H^2MM in matlab[56].
Importantly, throughout this work we make the clear distinction between sub-populations and states, where the latter is referred to the state models used to describe the dynamically interconverting sub-populations resolved from the data. This distinction is important, since thermodynamic states are single potential wells, and it is possible that the identified sub-populations are actually a group of states that interconvert much faster than the time resolution of the measurements.

2 Results

2.1 Verification of mpH^2MM against simulated data

Analysis with single parameter H^2MM (spH^2MM) and mpH^2MM can be performed using any given state model. Therefore, we must select the most likely state model among several, differing in their number of states and number of transition rate constants. Discriminating over- and under-fitted state models from the most likely model has proven difficult in the past[7, 73]. Previously, we proposed the modified Bayes information criterion (BIC'), which does not provide an extremum-based decision on the most likely state-model[7]. In the current work, we implement the integrated complete likelihood (ICL)[74, 75], which gets a minimum value for the most-likely state-model, as the primary criterion for state-model selection.
Using simulated smFRET data, where the ground truth of the number and properties of the states is known, we find that the selection of the most likely state model based on the ICL is more reliable than based on BIC' (see supplementary figure S2, and Jupyter notebooks in supplementary dataset[72]). Yet, there are instances in the simulated data, and in real data sets we describe later, where the the selection of the most likely state model based on ICL is of a model with too few states, relative to our prior knowledge of the system. Therefore, we always consider the ICL first, then BIC', and take into account the prior knowledge of the system when selecting the most likely state model (see supplementary section S2 for expanded discussion, supplementary figure S2).
To verify the validity of the multi-parameter approach, we perform a series of simple simulations (see supplementary Jupyter notebook mpH2MMsimulations[76]). We compare results of spH^2MM and mpH^2MM analyses of simulated data where the acceptor excitation photon stream was either included or excluded. Using this data, we find that selecting the most likely state model based on the ICL parameter reliably identifies the correct ground truth state-model, and this model accurately reproduces the transition rate constants, E_{raw} and S_{raw} values used in the simulation (supplementary figures S3,4, E_{raw}, supplementary table S1, S_{raw} values defined in supplementary equations S6 and S7, respectively). In contrast, spH^2MM is less reliable, and depending on the circumstances, it is unable to distinguish states with similar E_{raw} values, which are easily distin-

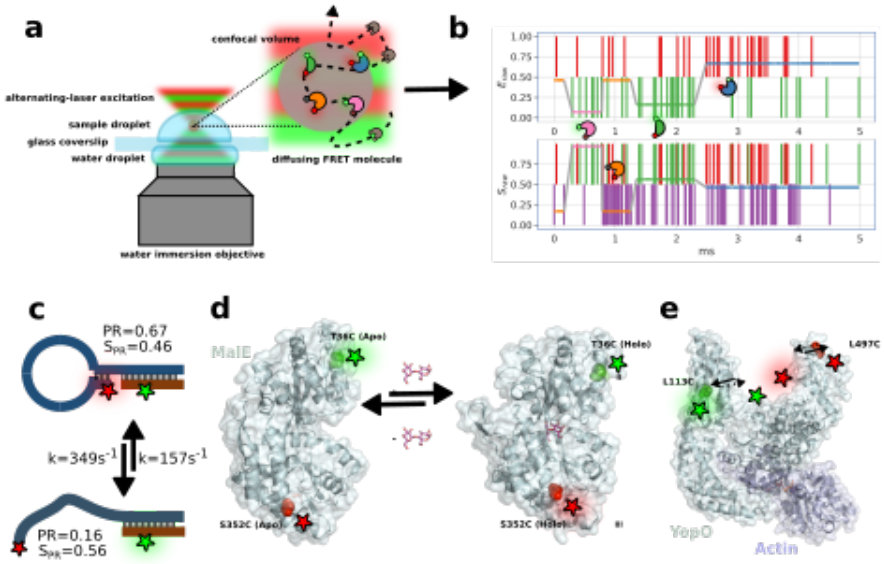

figure 1: **Cartoon representations of data acquisition, and biological systems examined in this work** a) Confocal microscope setup with inset illustrating the diffusive trajectory of a single molecule in and out of the confocal volume, undergoing conformational and photophysical changes, producing b) a photon time trace, photons represented by vertical bars, and the most likely state-path according to the *Viterbi* algorithm overlayed as horizontal colored line. c-e) Biological systems studied: c) DNA hairpin, d) maltose binding protein MalE conformational changes, and e) type III secretion effector YopO. See figure S1 for a version of this figure with transition rates, E_{raw} and S_{raw} values included for the biological systems.

guished in mpH^{2}MM by their S_{raw} values. Further, without the information about S_{raw}, interpretation of the models is more difficult, even if the correct number of states and their accurate E_{raw} values are recovered in spH^{2}MM.

2.2 DNA hairpin exhibiting millisecond dynamics

As a first biological test system for mpH^{2}MM, we used a DNA hairpin system introduced by Tsukanov *et al.* with a loop containing 31 adenines and a six base-pair stem[70]. The opening and closing rate constants of the hairpin vary as a function of the GC content of the stem as well as the sodium chloride (NaCl) concentration[70]. When appropriately labeled with a FRET donor and acceptor pair of dyes (ATTO 550 and ATTO 647N, respectively), the open and closed hairpin sub-populations exhibit distinct low and high mean E_{raw} values, respectively. The hairpin containing two GCs out of the six stem bases, which we term HP3, exhibited opening and closing rates of a few milliseconds, depending on the NaCl concentration in the buffer. Such a DNA construct with well-characterized and tunable transition rates serves as an ideal model system to test and characterize the performance of mpH^{2}MM.

We first perform nsALEX measurements[61] with this construct at a concentration of 300 mM NaCl, where a mix of both open and closed states are expected to interchange dynamically[70]. As a qualitative test for FRET dynamics occurring within bursts, we use burst variance analysis (BVA)[41], which compares the expected variance in E_{raw} based on shot noise (the static FRET semi-circle) against the actual variance in E_{raw}. BVA of the HP3 data shows clear deviation from the static FRET semi-circle, suggesting that individual HP3 molecules are undergoing FRET dynamics as they traverse the confocal volume, we term within-burst FRET dynamics (figure 2a). E-τ_D plots[44] also indicate within-burst dynamics (see supplementary figure S5). However, without the prior knowledge of the DNA hairpin behavior as a two-state FRET system, and without knowing how many more sub-populations unrelated to FRET may exist, it is not necessarily clear how many distinct sub-populations are involved in within-burst dynamics. In visual examination of the 2D E-S plot, three sub-populations are apparent: (i) an open hairpin sub-population with mean E_{raw} of 0.2, (ii) a closed hairpin sub-population, with a E_{raw} of 0.65, both open and closed sub-populations have mean S_{raw} of 0.5, and (iii) a third sub-population with a mean E_{raw} of 0, and mean S_{raw} of 1, where the acceptor is either in a dark state, or missing altogether (figure 2b). The 2D E-S plot also exhibits bursts with intermediate E_{raw} values, bridging between the open and closed hairpin sub-populations. As these bursts are particularly dynamic in the BVA analysis, these are bursts where the hairpin is undergoing opening and closing transitions while crossing the confocal volume.

Analyses of this data with spH^{2}MM and mpH^{2}MM show different patterns in the ICL values of the state-models. The ICL is minimized for spH^{2}MM models for a two-state model, while it is minimized for a four-state model when using mpH^{2}MM. Visual inspection of the one-dimensional projection of burst data onto the E_{raw} parameter immediately suggests an explanation for this dis-

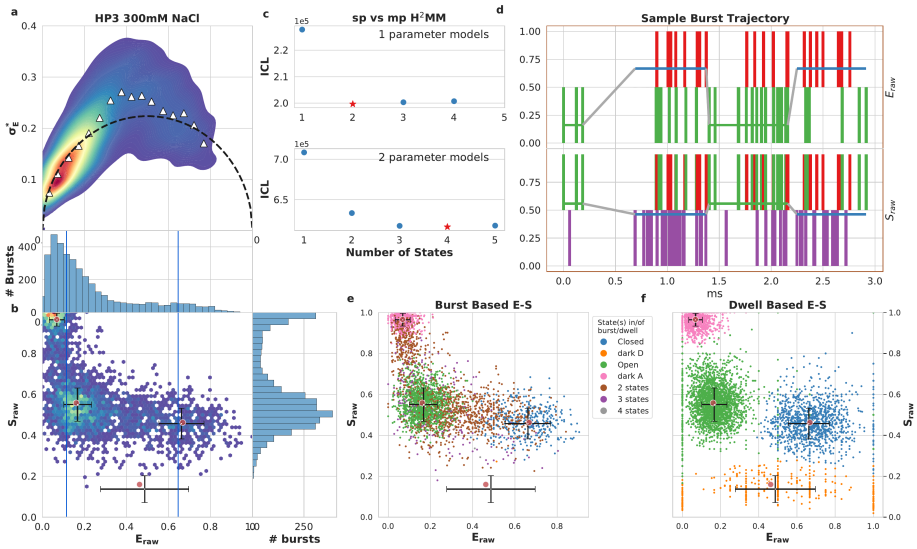

figure 2: **mpH^{2}MM results for DNA hairpin at 300 mM NaCl**. a) Burst variance analysis (BVA), the E_{raw} standard deviation of E_{raw} values of bursts is displayed versus their E_{raw} values. Bursts with E_{raw} standard deviations higher than expected solely from shot noise (semicircle), are ones that include dynamic heterogeneity, such as within-burst FRET dynamics. Triangles indicate the average of standard deviation values per E_{raw} bin. b) 2D histogram of E_{raw} and S_{raw} (E-S plots, colloquially) of bursts. The E_{raw} and S_{raw} values of sub-populations derived from mpH^{2}MM are marked by red circles, and the E_{raw} and S_{raw} standard deviation of these values, derived from the *Viterbi* dwell time analysis, are marked by black crosses. c) Comparison of values of the integrated complete likelihood (ICL) of spH^{2}MM (top panel) and mpH^{2}MM (bottom panel) of optimized models with different state-models. The most likely state-model is marked as a red star. d) A sample burst trajectory, with photons represented as colored vertical bars, with donor excitation photons colored green and red for donor and acceptor, respectively. Acceptor excitation photons are colored purple. E_{raw} (top panel) and S_{raw} (bottom panel) of sub-populations determined from dwells using the *Viterbi* algorithm, are overlayed on the photon bars, and colored to indicate the state of the dwell. The border color also represents the type of burst. e,f) E-S scatter plots of data processed by the *Viterbi* algorithm. Consecutive photons with the same state are considered as a single dwell, E_{raw} and S_{raw} values are then calculated as in equations S8 and S9, respectively. MpH^{2}MM-derived sub-populations and *Viterbi*-derived E_{raw} and S_{raw} standard deviations (SD) are overlayed as red circles and black crosses, respectively. e,f) E-S scatter plot of bursts (e) or dwells within bursts (f), color coded by which states are present in the bursts (e) or according to the state of the dwell (dwell based E_{raw} and S_{raw} defined in supplementary equations S8 and S9, respectively) (f), according to *Viterbi* algorithm. Color coding is the same throughout d, e and f. See supplementary figure S6 for more examples of bursts classified by the *Viterbi* algorithm. E-τ_D analysis is provided in supplementary figure S5.

crepancy, as it appears as only two sub-populations. The donor-only or dark-acceptor state, and the open hairpin state exhibit similar low E_{raw} values and are difficult to distinguish as sub-populations based solely on E_{raw}. This projection reflects the data accessible to spH^{2}MM, the donor excitation streams, and thus the open hairpin and dark acceptor states are expected to have nearly identical FRET signatures with regard to the streams accessible to spH^{2}MM, thus leading to the false inference of only two states. The open hairpin FRET sub-population and the dark-acceptor states are, however, quite distinct with regard to the acceptor excitation stream, which is accessible to mpH^{2}MM.
In the ICL-based selected four-state model retrieved by mpH^{2}MM, two out of the four states match nicely with the states in the ICL-based selected model from spH^{2}MM model, having similar E_{raw} values. Their S_{raw} values are $\sim$0.5 (figure 2b red circles), as expected for molecules undergoing FRET. The third and fourth states in the model can be matched to dark acceptor and dark donor sub-populations, respectively. The third state has a E_{raw} value $\sim$0 and a S_{raw} value $\sim$1 (figure 2b, top left red circle). This state has a clear sub-population of bursts associated with it in the 2D E-S plot. The state has an intermediate E_{raw} value, and a very low S_{raw} value of $\sim$0.17 (figure 2b, bottom red circle, supplementary table S2). There is no obvious sub-population visually observed in the E-S plots to which this would correspond, but the E_{raw} and S_{raw} values are consistent with this being a dark donor state. More importantly, comparing the parameters of the state models retrieved by spH^{2}MM and mpH^{2}MM, we find that the transition rate constants derived using mpH^{2}MM are closer to those found by Tsukanov *et al.*[70] than those extracted using spH^{2}MM (supplementary table S3, and supplementary .csv files of all state-models found by H^{2}MM analysis[72]). The transition rate constants provide a clue as to why the fourth state does not show up in the E-S plots as a distinct sub-population, as the transition rates predict rare transitions to it, and rapid transitions away from it. Thus, populating the fourth state occurs only briefly and rarely in bursts undergoing rapid dynamics, such that it does not appear as a clear sub-population in the E-S plots (supplementary table S3, and supplementary .csv file [72]).
The *Viterbi* algorithm finds the most-likely state path through each burst, given a state-model and its parameter values (figure 2d and supplementary figure S6a-e). We use this to classify bursts by which states are present within each burst (figure 2d, supplementary figure S6f), and separate photons into dwells, for which E_{raw} and S_{raw} can be defined (figure 2d, supplementary equations S8 and S9 in supplementary section S1.3). Additional analysis of dwells and their durations is provided in supplementary figures S7. Visual examination of the burst-based E-S plot (figure 2e) shows that the *Viterbi* algorithm reasonably classifies most bursts that have E_{raw} and S_{raw} values close to the predicted value of a given sub-population as only having that state present, as well as bursts with intermediate E_{raw} and S_{raw} that are predicted to include dwells of multiple states. Notably, there are only a few bursts classified as having dwells solely in the dark donor state (figure 2e), keeping with what is predicted by the transition rates, and indeed, few dwells are even found in this state (figure 2f, supplementary figure S6g). The scarcity of the donor dark state in the *Viterbi* analysis

serves to both confirm this observation and prove the sensitivity of mpH^{2}MM at the same time. In summary, using spH^{2}MM, we do not properly decouple the FRET-relevant information from the FRET-irrelevant dye transitions to fluorophore dark states for the DNA hairpin data, which influences the accuracy of the retrieved values for the E_{raw} and rate constant parameters. On the other hand, using mpH^{2}MM assists in the proper decoupling of the FRET-relevant information from the FRET-irrelevant ones and in gaining accurate parameter values. See supplementary figures S8-19 for additional hairpin data acquired at different concentrations of NaCl. Now that we have verified mpH^{2}MM with a well-defined biomolecular system of the DNA hairpin, HP3, we move to explore its usefulness in other biomacromolecular systems.

2.3 Quantifying the dynamics of a substrate-binding protein

In the previous example we examined a system that exhibits intrinsic conformational dynamics, hence dynamics that is not induced by binding of a ligand. Now, we test mpH^{2}MM on a system with conformational dynamics that is induced by substrate binding. For this we select the periplasmic maltose binding protein, MalE from *E. coli*[77], which is the extracellular component of the maltose ABC importer MalFGK$_2$-E[77]. MalE is a bilobed protein with a structural core built from a periplasmic binding protein (PBP)-like II domain. Two rigid domains, D$_1$ and D$_2$, are separated by a two-segment β-strand hinge and are complemented by a C-terminal embellishment that facilitates structural dynamics between open and closed states[17]. This allows for MalE to close upon substrate binding, similar to a venus fly-trap. For our nsALEX sm-FRET measurements we produced a MalE double-cysteine variant with labels at the outer sides of the two lobes, specifically residues T36C and S352C. As shown previously, this enables tracking of the opening and closing dynamics in single MalE molecules[17, 78]. We test three concentrations of the substrate maltose: none (apo), 1 µM (close to the K_D value[77]) and 1 mM (holo). FRET histograms, using a dual channel burst search (DCBS)[36] filter exhibit three sub-populations: (i) a minor, low E_{raw} sub-population at E_{raw} of 0.1, (ii) a major sub-population with an intermediate E_{raw} of 0.5, and (iii) a major sub-population with a high E_{raw} of 0.7. We use DCBS because the donor- and acceptor-only sub-populations are very strong, and otherwise overwhelm the nsALEX data. Since we apply DCBS, bursts of the high S_{raw} and low E_{raw} values cannot represent molecules with permanently dark acceptor, but could be the result of either a real conformation, or of frequent acceptor blinking. With increasing maltose concentration the fraction of the $\sim$0.5 E_{raw} sub-population decreases, while the fraction of the $\sim$0.7 E_{raw} sub-population increases (figure 3).

The BVA plot exhibits evidence of within-burst dynamics, so mpH^{2}MM analysis of within-burst dynamics is warranted (figure 3, top row).

In mpH^{2}MM analysis, the ICL-based model selection identifies the five-state model for 1 µM maltose, and the four-state model for 1 mM maltose. Ex-

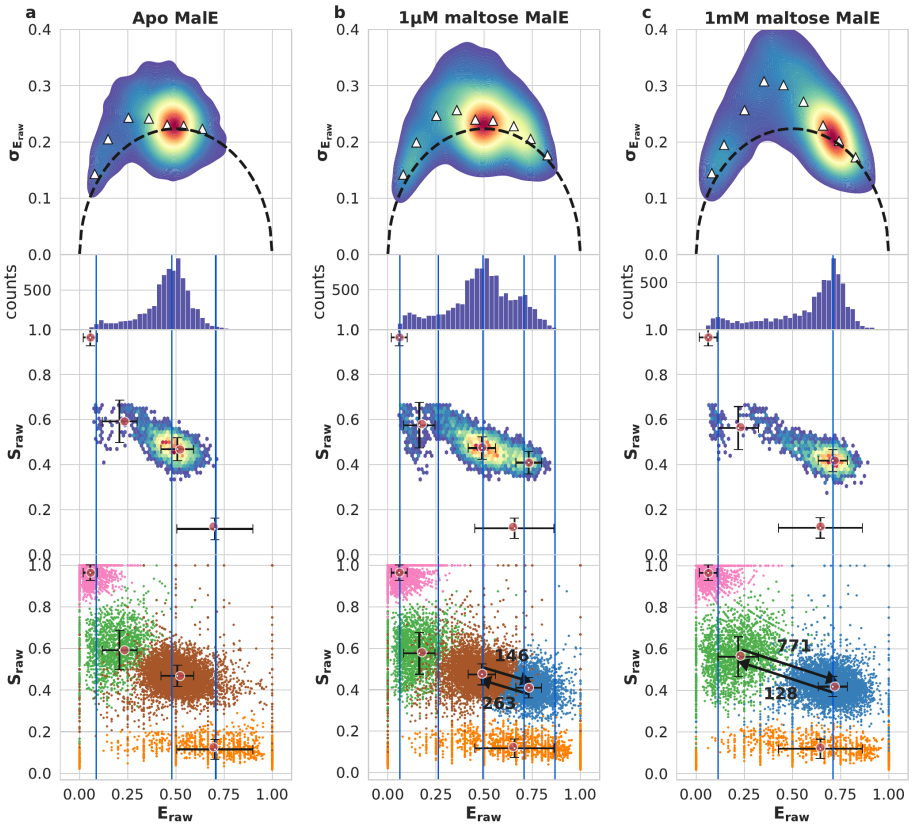

figure 3: **Results for MalE** Top row: BVA of concatenated dataset. Upper middle row: E_{raw} histogram of bursts. Lower middle row: E-S plot of bursts, with ICL-based selected results overlayed, red circles indicating the values derived from the ICL-based selected mpH^{2}MM state model, and the black crosses the standard deviation of the *Viterbi*-derived dwell E_{raw} and S_{raw} values. Vertical blue lines represent the E_{raw} values of the states from the ICL-based selected spH^{2}MM state model. Bottom row: Dwell-based E-S plots as in figure 2, with transition rates (in units of s^{-1}) between selected states indicated by arrows added. a) apo MalE, b) 1 µM maltose, c) 1 mM maltose.

amining these models, we find that all contain a single high S_{raw} state and a single low S_{raw} state, with the high S_{raw} state also having an E_{raw} of 0, and importantly, no bursts exist in these ranges due to the use of a DCBS filter (supplementary tabels S4 and S5). Therefore, we can conclude that these states are the result of transition in the donor and acceptor dyes for the low and high S_{raw} states, respectively. The transition rates of the models and *Viterbi* analysis both show that these states are appreciably populated (figure 3, bottom row, supplementary figures S20-22, supplementary table S7, and supplementary .csv file [72]), thus the use of mpH^{2}MM analysis is vital here. Depending on the maltose concentration, the ICL of spH^{2}MM analysis predicts different numbers of states for each concentration, and the E_{raw} values of the states within these models are far less consistent (figure 3, vertical bars). These states are often similar to states found by mpH^{2}MM, but their interpretation would be ambiguous if we did not have mpH^{2}MM for additional information. In other cases, spH^{2}MM-based states appear as a fusion of two states found by mpH^{2}MM.
As another example of how vital mpH^{2}MM analysis is in this case, consider the BVA signature of the apo form. Our analysis shows that the FRET dynamics for E_{raw} is not due to the actual dynamics between the open conformations of MalE. This is clear since the $\sim$0.7 E_{raw} sub-population is not identified if maltose is not supplied. Such interpretation cannot be made from spH^{2}MM results, due to the less consistent prediction of the number of states, and the parameters of those models. Therefore, we can confirm that MalE undergoes conformational dynamics linked to its function, solely induced by the binding of maltose, hence it follows an induced-fit binding mechanism.

2.4 Adapting to µsALEX: microsecond dynamics of YopO

Finally, we demonstrate how to apply mpH^{2}MM with µsALEX experiments. For this we use the type-III secretion effector from *Yersinia* species, YopO[71]. We measure the conformational dynamics of a double-cysteine variant of YopO, with dyes labeling residues L113C and L497C. These labelling positions are expected to change distances upon binding to actin. Burst selection is performed using the DCBS filter, for the same reasons as in the MalE data - there are strong blinking dynamics that overwhelm the analysis otherwise. Interestingly, in the absence of actin there appears to be a single FRET sub-population in E-S plots, with tails towards dark donor and dark acceptor sub-populations. Nevertheless, BVA shows these bursts have a variance above the expected static FRET semi-circle (figure 4a, top panel), and hence within-burst dynamics. In the presence of bound actin (60 µM), a main sub-population is present with a shift toward lower E_{raw} values, and the BVA plot suggests no signature of within-burst dynamics at that main sub-population (figure 4b, top panel).
Using this µsALEX data with mpH^{2}MM, the alternation period proves to be an obstacle, causing mpH^{2}MM analysis to fail without a key adjustment to the data. Unlike in nsALEX, multiple photons can be detected during a given alternation period of the donor or acceptor excitation lasers. This results in photons originating from donor excitation that are temporally separated from

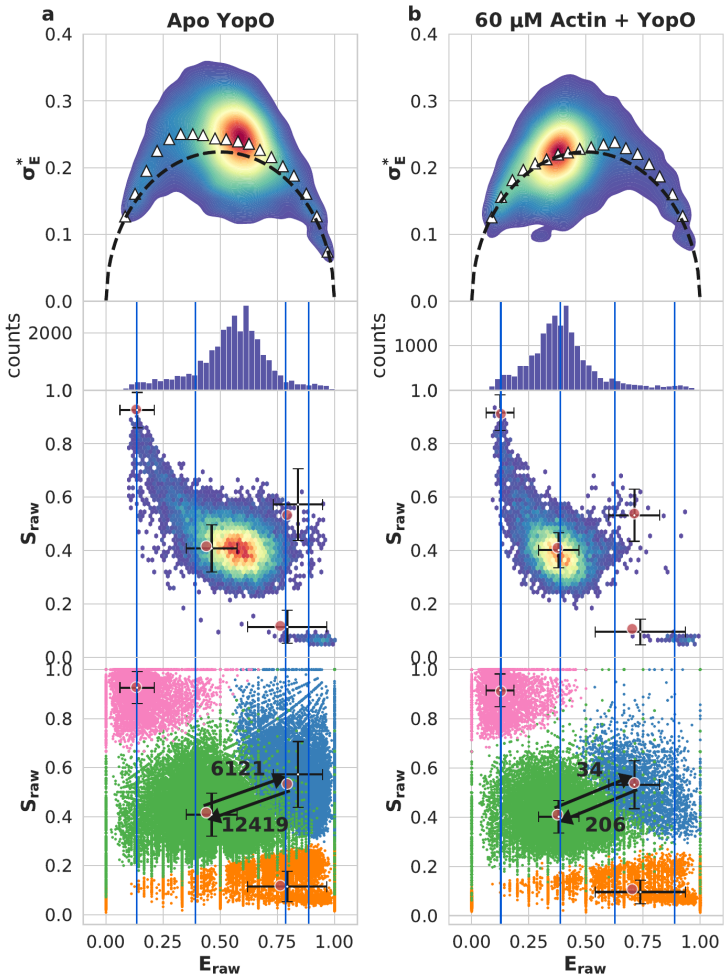

figure 4: **Results for YopO** a,b) Top row: BVA analysis. Upper middle row: E_{raw} histogram of bursts, lower middle row: E-S plot of bursts. Red dots indicate mpH^{2}MM states. Bottom row: Dwell-based E-S plots as in figure 2, with transition rates (in units of s^{-1}) between selected states indicated by arrows added. Vertical bars indicate the E_{raw} values of the states for the BIC'-based spH$_{\mathrm{Eraw}}$ model. a) apo YopO exhibiting sub-millisecond dynamics. b) YopO with 60 µM actin exhibiting slower within-burst dynamics, and a shift towards the lower FRET conformation.

photons originating from acceptor excitation in a periodic pattern, resulting in alternating periods where no photons originating from donor excitation are detected, and alternatively periods where no photons originating from acceptor excitation are detected. When we first apply mpH^{2}MM to µsALEX data, we find that instead of detecting states with meaningful S_{raw} values, all states have S_{raw} values of either 0 or 1, and transition rates are all very similar to the alternation rate, meaning that mpH^{2}MM detects the alternation rate instead of meaningful dynamics (supplementary figure S23a,b).
To enable meaningful µsALEX analysis via mpH^{2}MM that incorporates photons originating from acceptor excitation, we introduce a shift so that the times of the acceptor excitation photons overlap with the photons originating from donor excitation (see supplementary section S1.1.1). By doing so, the alternation period is no longer detected and meaningful dynamics with E_{raw} and S_{raw} values can be recovered (figure 4, supplementary figure S23c). The usefulness of this analysis is evidenced by the detection of dark donor and dark acceptor states. Thus application of mpH^{2}MM even to µsALEX data usually yields better results than with spH^{2}MM. However, caution must be taken to avoid artefacts due to the alternation period. For instance, if the time-scale of a transition approaches that of the alternation period, S_{raw} values may be biased or averaged together due to the shift (for in-depth discussion on this topic, see supplementary section S1.1.2).
Applying mpH^{2}MM to analyze the measured data of YopO in the presence of actin, the most likely model is clearly a four-state model, using an alternation period of 50 µs (20 kHz alternation rate). The ICL-based model selection identifies four states, while the BIC'-based selection shows the four-state model to be close to the 0.005 threshold, and the five-state model can be further disregarded based on its reasonableness. Selection is more difficult for the apo results, as the two criteria disagree with ICL-based model selection that identifies three states and BIC'-based model selection that identifies five. Therefore, the most likely model is either the three-, four-, or five-state model, and examination of these models and prior knowledge of the data is necessary. The three-state model predicts states that appear as dark donor and acceptor, and a single FRET state. This model can be ruled out because the BVA shows significant dynamics around the single FRET population, and thus the single FRET state is insufficient to explain the BVA signature. The five-state model on the other hand suffers from the opposite problem - there are two states with very low S_{raw} values, where it appears as though the dark donor state has split into two. The four-state model, however, is reasonable, showing two FRET states, dark donor and dark acceptor states (supplementary tables S6 and S7). Transition rates between the high and low FRET states are 12,400 s^{-1} and 6,000 s^{-1} for transitions from high E_{raw} to low E_{raw} states, and for transitions from low E_{raw} to high E_{raw} states, respectively. These dynamics, however, approach the timescale of the alternation rate (20 kHz; for detailed discussion and examination see supplementary section S1.1.2 as well as supplementary figures S24 and S25). Based on the analyses of the *Viterbi*-derived dwell times, error analysis of data subsamples, and comparison with the results of mpH^{2}MM analysis employed on

other measurements using different alternation periods, we conclude that these transition rates are not artefacts, and reflect true FRET transitions in the data (see supplementary section S1.1.2, supplementary figures S26-28 for comparison of alternation periods, supplementary tables S8 and S9 for optimized model of different alternation period).
The timescale of the FRET dynamics being faster than burst duration by two orders of magnitude explains the appearance of the data in the FRET histogram as a single FRET population, with yet a signature of within-burst dynamics in the BVA plot. Inspecting the results of the mpH^{2}MM analysis, the meaning of the within-burst FRET dynamics of YopO in the absence of actin becomes clear - it exhibits transitions in the tens of microseconds between two main FRET states intertwined with rapid transitions to dark donor and dark acceptor states. Each burst that lasts a few milliseconds contains multiple dwells in the underlying states and transitions between them, and so the bursts are averaged-out as a single main population. When comparing these results, with the analysis results of YopO in the presence of bound actin, it becomes clear that the lower E_{raw} state of the two FRET states in the absence of actin is stabilized upon actin binding. Therefore, we can conclude that YopO conformational dynamics relevant to actin binding occurs intrinsically, regardless of the presence of actin, and that actin stabilizes and locks one of the pre-existing conformations.
Without using mpH^{2}MM, it would have been difficult to accurately report on this dynamics, as the FRET within-burst dynamics is intertwined with FRET-irrelevant transitions to dark states. It should be noted that we have successfully decoupled conformational and photophysical dynamics in µsALEX data without the use of fluorescence lifetimes.

3 Discussion and Conclusions

MpH^{2}MM increases both the information content of the results and the sensitivity of the H^{2}MM algorithm to differences in the photon streams that are too subtle when examining only a single parameter. We have shown that mpH^{2}MM is able to disentangle dark acceptor states from low FRET states that have structural meaning. We have exhibited the advantage of using mpH^{2}MM to elucidate an accurate quantitative picture on two proteins with two types of conformational dynamics that serve their function: 1) MalE with conformational dynamics induced by maltose binding, and 2) YopO with conformational dynamics occurring intrinsically, and upon actin binding one of the conformational states get stabilized. In both cases the overall picture is complicated by having the FRET-relevant transitions intertwined with the FRET-irrelevant dye transition to dark states, and not taking these into account could result in wrongly elucidated quantities and potentially wrong interpretations. Of note is the rapid conformational dynamics on the order of tens of microseconds in YopO when actin was absent. The exact description of the dynamics was possible using mpH^{2}MM on µsALEX, and hence did not necessarily require analysis of the correlation of donor fluorescence lifetimes with ratiometric FRET values, as can

be done using FRET lines fits to E-τ_D 2D plots in lifetime-based smFRET[44]. As µsALEX and nsALEX setups are now commonly used, the acceptor excitation stream is usually available, therefore, mpH^{2}MM maximizes the use of available data for characterizing rapidly interconverting sub-populations.

MpH^{2}MM is therefore a powerful tool for the quantification of rapid conformational dynamics in a variety of systems, while also extracting information that can be used to extract inter-dye distance distributions. The integration of the acceptor excitation photon stream is critical in this process, as we have shown that spH^{2}MM often conflates photophysical and conformational states, leading to incorrect E_{raw} and transition rate constants. Comparing a given protein or other biomacromolecular system with different ligands, or concentrations of ligands, it is possible to discriminate when a system demonstrates intrinsic conformational dynamics or conformational changes triggered by ligands. MpH^{2}MM provides accurate quantitative measures of both transition rates and mean E_{raw} values, the latter of which can be converted into accurate mean FRET efficiency values with the proper correction factors for the system[79]. Such information can then be converted into mean inter-dye distances, which provide invaluable information for FRET-based integrative structural models[7, 33, 79].

We have demonstrated mpH^{2}MM with nsALEX and µsALEX measurements, but it is by no means restricted to these two-detector setups. The most obvious application of mpH^{2}MM beyond ALEX, is with the multiple photon streams in multi-parameter fluorescence detection (MFD)[34, 43], or with multi-color smFRET-based measurements[62–69]. Here, three or even four spectrally-distinct dyes are attached to the biomolecule of interest, and each produces a distinct photon stream. This enables the simultaneous observation of multiple inter-dye FRET efficiencies at once. If qualitative tests indicate that such a system is undergoing within-burst dynamics, mpH^{2}MM is well-suited to extract the transfer efficiencies relevant to the underlying dynamically-interconverting sub-populations. Applying these methods is as simple as assigning an index to each photon stream. We include a supplementary Jupyter notebook using a developer version of FRETBursts[80] that accepts fluorescence anisotropy information from multi-parameter fluorescence detection, or from MFD coupled to pulsed-interleaved excitation[34, 43], and demonstrate mpH^{2}MM's ability to disentangle fluorescence anisotropies. Values within the emission probability matrix can then be used as intensities to calculate all relevant ratiometric values. Multiple conformational sub-populations interconverting at sub-millisecond timescales could be simultaneously measured and disentangled with such a setup. Information on fluorescence anisotropy could also be incorporated, which, depending on the labelling scheme could report on dye steric restriction or oligomeric state of the system in question.

In this work we used two ratiometric parameters drawn from ratios of photon counts of the photon streams available in ALEX-based measurements within the mpH^{2}MM framework. In some smFRET measurements, such as in nsALEX, the photon nanotimes, which are the basis for fluorescence lifetime data, can also be considered as a parameter within the mpH^{2}MM framework. However, unlike E_{raw} and S_{raw}, which are approximately binomially-distributed, photon

nanotimes distribute exponentially or sometimes according to a sum of exponentials. To transform photon nanotime data into a parameter that is also centrally distributed, and hence one that can be used within the mpH^{2}MM framework, we propose a method for mapping the non-binomially distributed lifetime to a binomially-distributed parameter amenable to mpH^{2}MM (see supplementary section S3 for further details).
The new H2MM_C python package makes H^{2}MM analysis much more practical, most analysis, for up to six states, take less time than the data acquisition times, given our modest hardware (a two year old middle-tier gaming laptop). See supplementary section S4 and supplementary tables S10,11 for system requirements and the duration of calculations in this paper. The supplied Jupyter notebooks provide examples for how to execute mpH^{2}MM using FRETBursts. Experimenters using other platforms must utilize their knowledge of the fine details of their data to properly filter and cast their data into the simple and general format that the H2MM_C package[76] accepts. We also provide an in depth tutorial available on Zenodo[81].

4 Methods

4.1 Production of YopO and MalE variants

The double-cysteine variant YopO L113C/L497C is produced and purified as described in Peter *et al.*[71] and kindly provided by Gregor Hagel uken and Martin Peter, Institute of Structural Biology (University of Bonn). The double-cysteine variant MalE T36C/S352C is generated and purified according to methods reported previously[17].

4.2 Labeling of MalE

The MalE variant T36C/352C is stochastically-labelled with Alexa Flour™555 and Alexa Fluor™647 dye derivatives as described in Peter *et al.* and deBoer *et al.*[17, 82]. The His$_6$-MalE double variant (200 µg) is incubated with 1 mM DTT and loaded immediately after on 200 µL (wet volume) Ni-Sepharose 6 Fast Flow resin, pre-equilibrated with labelling buffer 1 (50 mM Tris-HCl pH 7.4, 50 mM KCl). After a washing step with 50 column volumes labelling buffer 1, the loaded resin is incubated overnight at 4°C with 5-fold excess (25 nmol of each fluorophore dissolved in 1 mL of labelling buffer 1. Next, the resin is further washed with 50 column volumes labelling buffer 1 to remove the excess unbound fluorophores. Labelled protein is eluted with 800 µL elution buffer (50 mM Tris-HCl pH 8.0, 50 mM KCl, 500 mM imidazole) and further purified by size-exclusion chromatography (ÄKTA pure system, Superdex 75 Increase 10/300 GL column, GE Healthcare). Protein concentration is determined using the protein extinction coefficient and corrected for direct absorption of the fluorophores at 280 nm. Labelling efficiencies are estimated to be at least 60 % for each fluorophore individually and donor-acceptor pairing at least 20 %.

Labeled MalE is stored in 50 mM Tris-HCl pH7.4, 50 mM KCl and 1 mg mL^{-1} bovine serum albumin (BSA) at 4°C for no more than 3 days. Concentrations ranged between 10 to 100 nM.

4.3 Labeling of YopO

The protein variant YopO L113C/L497C is stochastically-labelled with fluorophore-linked maleimide derivatives, as described previously[82]. Briefly, 200 µg of protein is incubated with 5 mM DTT at 4°C for 30 minutes, to prevent oxidation of the cysteine thiol groups. The protein is loaded onto a PD Mini-Trap G-25 column (GE Healthcare) pre-equilibrated with Buffer A (50 mM Tris-HCl pH 7.4, 50 mM KCl) and subsequently eluted with 1 mL of Buffer A by gravity gel filtration, in order to eliminate the excess of DTT. The eluted protein is incubated overnight at 4°C with 50 nmol, respectively, of Alexa Fluor™555- and Alexa Fluor™647- C_2 maleimide (ThermoFisher Scientific). Excess dyes are removed again by gravity gel filtration using a PD Min-Trap G-25 column, as described above. The labelled protein is further purified from residual dyes and soluble aggregates by size-exclusion chromatography (SEC), with a Superdex™75 Increase 10/300 GL column, on an ÄKTA pure system (GE Healthcare). Protein concentration is determined using the protein extinction coefficient and corrected for direct absorption of the fluorophores at 280 nm.
Labelling efficiencies are estimated to be at least 60 % for each fluorophore individually and donor-acceptor pairing at least 20 %.

4.4 Experimental setup

4.4.1 Experimental Setup for Studies of HP3

We performed the nsALEX smFRET measurements of the doubly-labeled DNA hairpin construct[70] in the presence of 50, 100, 200, 250, 300 and 350 mM sodium chloride, using a confocal-based setup (ISS™, USA) assembled on top of an Olympus IX73 inverted microscope stand. We use a pulsed picosecond fiber laser (λ=532 nm, pulse width of 100 ps FWHM, operating at 20 MHz repetition rate and 100 µW measured at the back aperture of the objective lens) for exciting the Cy3B donor dye (FL-532-PICO, CNI, China), and a pulsed picosecond diode laser (λ=642 nm, pulse width of 100 ps FWHM, operating at 20 MHz repetition rate and 60 µW measured at the back aperture of the objective lens) for exciting the ATTO 647N acceptor dye (QuixX® 642-140 PS, Omicron, GmbH), delayed by 25 ns. The laser beams pass through a polarization-maintaining optical fiber and then further shaped by a linear polarizer and a halfwave plate. A dichroic beam splitter with high reflectivity at 532 and 640 nm (ZT532/640rpc, Chroma, USA) reflects the light through the optical path to a high numerical aperture (NA) super apochromatic objective (60X, NA=1.2, water immersion, Olympus, Japan), which focuses the light onto a small confocal volume. The microscope collects the fluorescence from the excited molecules through the same objective, and focuses it with an achromatic lens (f = 100 mm) onto a 100 µm diameter

pinhole (variable pinhole, motorized, tunable from 20 µm to 1 mm), and then re-collimates it with an achromatic lens (f = 100 mm). Then, donor and acceptor fluorescence are split between two detection channels using a dichroic mirror with a cutoff wavelength at λ=652 nm (FF652-Di01-25x36, Semrock Rochester NY, USA). We further filter the donor and acceptor fluorescence from other light sources 585/40 nm (FF01-585/40-25, Semrock Rochester NY, USA) and 698/70 nm (FF01-698/70-25, Semrock Rochester NY, USA) band-pass filters, respectively, and detect the donor and acceptor fluorescence signals using two hybrid photomultipliers (Model R10467U-40, Hamamatsu, Japan), routed through a 4-to-1 router to a time-correlated single photon counting (TCSPC) module (SPC-150, Becker & Hickl, GmbH) as its START signal (the STOP signal is routed from the laser controller). We perform data acquisition using the VistaVision software (version 4.2.095, 64-bit, ISS^{TM}, USA) in the time-tagged time-resolved (TTTR) file format. After acquiring the data, we transform it into the photon HDF5 file format[83] for easy dissemination of raw data to the public, and easy input in the FRETBursts analysis software.

4.4.2 Experimental Setup for Studies of MalE

The nsALEX measurements on MalE are performed using a home-built setup, assembled around an Olympus IX73 inverted microscope stand. We use a picosecond pulsed diode laser (λ=532 nm, pulse width of 100 ps FWHM, operating at 20 MHz repetition rate and 32 µW at the back aperture of the objective) for exciting the Alexa Fluor™555 donor (LDH-P-FA-530B, Picoquant GmbH), and a picosecond pulsed diode laser (λ=640 nm, pulsewidth of 90 ps FWHM, operating at 20 MHz repetition rate, and 20 µW at the back aperture of the objective) to excite the Alexa Fluor™647 acceptor (LDH-D-C-640, Picoquant, GmbH), driven by the same PDL828 "Sepia II" (Picoquant, GmbH) controller. The laser light is guided into the microscope by a dual-edge beamsplitter (ZT532/640rpc Chroma/AHF, GmbH) and focused to a diffraction-limited excitation spot by an oil immersion objective (UPLSAPO 60XO, Olypus). The emitted light is collected through the same objective, spatially filtered through a 50 µm pinhole, and spectrally split into donor and acceptor channels by a single-edge dichroic mirror (H643 LPXR, AHF). The emission is filtered (donor: BrightLine HC 582/75, Semrock/AHF, acceptor: Longpass 647 LP Edge Basic, Semrock/AHF) and the signal is recorded with avalanche photodiodes (SPCM-AQRH-34, Excelitas) and a TCSPC module (HydraHarp400, Picoquant, GmbH).
Coverslips are passivated with 1 $mg\,mL^{-1}$ BSA in PBS buffer before adding around 100 µL of sample. MalE stock solution is diluted to ∼50 pM concentration in 50 mM Tris-HCl pH 7.4, 50 mM KCl, and either, none, 1 µM or 1 mM of the ligand maltose.

4.4.3 Experimental Setup for Studies of YopO

The µsALEX measurements of YopO are performed using the setup in Gebhardt*et al.*[84]. These are conducted on the same home-built microscope as the

MalE experiments, built around an Olympus IX71 base, although the lasers and dichroics are replaced as described below. We use a continuous wave λ=532 nm diode laser (OBIS 532-10-LS, Coherent, USA) laser with 60µW power measured at the back aperture of the objective to excite the donor Alexa Fluor™555 dye, and a continuous wave λ=640 nm diode laser (OBIS 640-100-LX, Coherent, USA) with 25µW power measured at the back aperture of the objective. The lasers are distally modulated by TTL pulses with an alternating frequency of 10 kHz, 20 kHz, and 100 kHz, for an alternation period of 100 µs 50 µs, and 10 µs, respectively. The lasers are combined and coupled into a polarization maintaining single-mode patch cable (P-3-488PM-FC2, Thorelabs, USA). The laser light is reflected into the objective by a dual-edge dichroic mirror (ZT532/640rpc, Chroma/AHF) and focused by a water immersion objective (UPlanSApo 60/1.2w, Olympus, GmbH). The dichroic mirrors, fluorescent filters and avalanche photodiodes are identical to those used for acquisiton of MalE data.
Coverlips are passivated with BSA as in MalE measurements. 100 µL of YopO solution, diluted to between 50 pM and 80 pM is used for each measurement in 50 mM Tris-HCl pH 7.4, 50 mM KCl. For measurements with actin, the buffer also contained 50 µM non-muscle human actin protein (Cytoskeleton, Inc) and 0.2 mM ATP and 0.2 mM $CaCl_2$.

4.5 Burst Selection

All data processing and analysis is performed using Jupyter Notebooks available in supplementary dataset, along with the accompanying photon-HDF5 files containing the raw data[72]. We perform burst search and selection using the FRETBursts analysis software[85]. Background is assessed per each 30 seconds of acquisition, and bursts are identified as time periods were the instantaneous photon count rate of a sliding window of $m = 10$ consecutive photons is at least $F = 6$ times higher than the background rate. Bursts in the normal selection are selected if they include at least 30 photons in total between all streams. Visualizations are performed using FRETBursts' dplot function, or matplotlib when greater customization is desired.

4.6 Single and Multi-parameter H^2MM analysis

Bursts identified by FRETBursts are then converted into a format readable by the H2MM_C software[76], by a simple function supplied in the Jupyter notebooks available in supplementary dataset[72], this function is also responsible for applying the shift to acceptor excitation photons in µsALEX experiments (supplementary section S1.1.1). In spH^2MM, only photons arising from donor excitation are considered, assigned to either donor or acceptor streams, identified by index 0 or 1, respectively, depending on at which detector they arrived. MpH^2MM also considers photons arriving during acceptor excitation, assigning these photons an index of 2. All H^2MM calculations are performed within the Jupyter notebooks, available in supplementary dataset[72], using the Python

package by Paul David Harris[76]. We use the H^{2}MM algorithm (both single- and multi-parameter) to test how well different state-models describe the data.

4.6.1 Model Selection

To choose the best model, we primarily use the ICL[74, 75], where the state-model reaching a minimal ICL is generally considered the one that describes the data best, with minimal free parameters. We always calculate sufficient numbers of state models to ensure ICL is minimized. The ICL parameter is defined in Eq. 1:

$$ICL(m) = -2\ln(\mathbf{p}(\mathbf{y}, \hat{\mathbf{s}}|m, \hat{\lambda_m})) + K\ln(n) \tag{1}$$

where $\ln(\mathbf{p}(\mathbf{y}, \hat{\mathbf{s}}|m, \hat{\lambda_m}))$ is the posterior probability of the most likely state path, as determined by the *Viterbi* algorithm, K is the number of free parameters in the model, and n is the number of photons in all bursts in the data set. K is calculated as in Eq. 2:

$$K = q^2 + (r-1)q - 1 \tag{2}$$

where q is the number of states the state-model represents, and r is the number of photon streams used for the calculation of all of the parameters that are assessed. For spH^{2}MM, $r = 2$, while for nsALEX mpH^{2}MM, $r = 3$. The ICL is preferable as an extremum-based criterion over the previously proposed threshold based on the modified Bayes Information Criterion (BIC')[7]. See supplementary dataset[72] for Jupyter notebooks testing the reliability of ICL with simulated data sets generated using PyBroMo[86] (https://github.com/OpenSMFS/PyBroMo/releases/tag/0.8.1; was utilized in previous works[7, 83, 87]). We use the *Viterbi* algorithm to find the most likely state path based on the posterior probability.

4.6.2 *Viterbi* Analysis

From the state path, photons are separated into dwells, each of which can be assigned a duration, a mean E_{raw}, and for mpH^{2}MM, a mean S_{raw}. This also allows bursts to be classified by which and how many states are present. As one measure of error, we use the weighted standard deviation and the weighted standard error of the E_{raw} and S_{raw} as a proxy for the standard error of the H^{2}MM model (see supplementary section S1.3 for full derivation).

4.6.3 Error Analysis by Variance of Subsets

Analysis of the variance of subsets is another method to assess the error of parameters (see supplementary information section S1.4 for detailed description). This is implemented as a function in the Jupyter notebooks in the supplementary dataset[72]. This is an attractive approach, as it does not depend on any most likely state-path like in the *Vieterbi* based approach. This method, however, is significantly more computationally expensive than the *Viterbi* approach.

5 Data Availability

The photon-HDF5 files, and accompanying Jupyter notebooks used for analyzing the photon-HDF5 files during the current study are available in the Zenodo Repository with the identifier DOI: 10.5281/zenodo.5566809 e.g. https://zenodo.org/record/5566809 [72], H2MM_C code is available on github with the identifier DOI: 10.5281/zenodo.5535302 e.g. https://github.com/harripd/H2MMpythonlib [76].

6 Author Contributions

E.L. performed HP3 nsALEX measurements. C.G. performed MalE nsALEX measurements. A.N. and T.C. performed YopO µsALEX experiments. P.D.H. analyzed data and contributed analytical tools. P.D.H. & E.L. designed and performed the research and composed the initial manuscript. P.D.H., A.N., C.G., T.C., S.W. & E.L. discussed the data and contributed to the final version of the manuscript.

7 Acknowledgements

We thank Greggor Hagel ucken and Martin Peter from the Institute of Structural Biology (University of Bonn, GER) for providing YopO. We would like to thank Robert Quast and Emmanuel Margeat for insightful discussions regarding the implementation of mpH^{2}MM for the analysis of 4-detector nsALEX measurements (2-color smFRET, with fluorescence anisotropies). This paper was supported by the National Institutes of Health (NIH, grant R01 GM130942 to S.W. and E.L. as a subaward), the National Science Foundation (NSF, grants 1818147 and 1842951 to S.W.), the Human Frontiers Science Program (HFSP, grant RGP0061/2019 to S.W.), the Israel Science Foundation (ISF, grant 3565/20 to E.L., within the *KillCorona* – Curbing Coronavirus Research Program), the Milner Fund (to E.L.), and the Hebrew University of Jerusalem (start-up funds to E.L.). Work in the lab of T.C. was financed by Deutsche Forschungsgemeinschaft (SFB863, project A13 and GRK2062, project C03), an ERC Starting Grant (No. 638536 – SM-IMPORT to T.C.) and by the Center of Nanoscience Munich (CeNS). We would also like to acknowledge the great help of Bill Harris in making the H2MM_C package cross platform.

References

[1] Eitan Lerner et al. "Toward dynamic structural biology: Two decades of single-molecule Förster resonance energy transfer". In: *Science* 359.6373 (Jan. 2018), eaan1133. ISSN: 0036-8075. DOI: 10.1126/science.aan1133. URL: https://www.sciencemag.org/lookup/doi/10.1126/science.aan1133.

[2] Eitan Lerner et al. "FRET-based dynamic structural biology: Challenges, perspectives and an appeal for open-science practices". In: *eLife* 10 (2021), e60416. DOI: 10.7554/eLife.60416.

[3] Benjamin Schuler and Hagen Hofmann. "Single-molecule spectroscopy of protein folding dynamics-expanding scope and timescales". In: *Current Opinion in Structural Biology* 23.1 (2013), pp. 36–47. ISSN: 0959440X. DOI: 10.1016/j.sbi.2012.10.008. URL: http://dx.doi.org/10.1016/j.sbi.2012.10.008.

[4] Haim Yuval Aviram et al. "Direct observation of ultrafast large-scale dynamics of an enzyme under turnover conditions". In: *Proceedings of the National Academy of Sciences* 115.13 (Mar. 2018), pp. 3243–3248. ISSN: 0027-8424. DOI: 10.1073/pnas.1720448115. URL: http://www.pnas.org/lookup/doi/10.1073/pnas.1720448115.

[5] Hisham Mazal and Gilad Haran. "Single-molecule FRET methods to study the dynamics of proteins at work". In: *Current Opinion in Biomedical Engineering* 12 (2019), pp. 8–17. DOI: 10.1016/j.cobme.2019.08.007.

[6] Nicole C Robb et al. "The Transcription Bubble of the RNA Polymerase – Promoter Open Complex Exhibits Conformational Heterogeneity and Millisecond-Scale Dynamics : Implications for Transcription Start-Site Selection". In: *Journal of Molecular Biology* 425.5 (2013), pp. 875–885. ISSN: 0022-2836. DOI: 10.1016/j.jmb.2012.12.015. URL: http://dx.doi.org/10.1016/j.jmb.2012.12.015.

[7] Eitan Lerner, Antonino Ingargiola, and Shimon Weiss. "Characterizing highly dynamic conformational states: The transcription bubble in RNAP-promoter open complex as an example". In: *The Journal of Chemical Physics* 148.12 (Mar. 2018), p. 123315. ISSN: 0021-9606. DOI: 10.1063/1.5004606. URL: http://dx.doi.org/10.1063/1.5004606%20http://aip.scitation.org/doi/10.1063/1.5004606.

[8] Michele Cristóvão et al. "Single-molecule multiparameter fluorescence spectroscopy reveals directional MutS binding to mismatched bases in DNA". In: *Nucleic Acids Research* 40 (12 2012), pp. 5448–5464. DOI: 10.1093/nar/gks138.

[9] Tomas Fessl et al. "Dynamic action of the Sec machinery during initiation, protein translocation and termination". In: *eLIFE* 7 (2018), e35112. DOI: 10.7554/eLife.35112.

[10] Antonio N. Calabrese et al. "Inter-domain dynamics in the chaperone SurA and multi-site binding to its outer membrane protein clients". In: *Nature Communications* 11 (2020), p. 2155. DOI: 10.1038/s41467-020-15702-1.

[11] Hisham Mazal et al. "Tunable microsecond dynamics of an allosteric switch regulate the activity of a AAA+ disaggregation machine". In: *Nature Communications* 10 (2019), p. 1438. DOI: 10.1038/s41467-019-09474-6.

[12] Yongfang Zhao et al. "Single-molecule dynamics of gating in a neurotransmitter transporter homologue". In: *Nature* 465.7295 (Mar. 2010), pp. 188–193. ISSN: 0028-0836. DOI: 10.1038/nature09057. URL: http://www.nature.com/articles/nature09057.

[13] Yongfang Zhao et al. "Substrate-modulated gating dynamics in a Na+-coupled neurotransmitter transporter homologue". In: *Nature* 474.7349 (June 2011), pp. 109–113. ISSN: 0028-0836. DOI: 10.1038/nature09971. URL: http://www.nature.com/articles/nature09971.

[14] Guus B. Erkens et al. "Unsynchronised subunit motion in single trimeric sodium-coupled aspartate transporters". In: *Nature* 502.7469 (Oct. 2013), pp. 119–123. ISSN: 0028-0836. DOI: 10.1038/nature12538. URL: http://www.nature.com/articles/nature12538.

[15] Giorgos Gouridis et al. "Conformational dynamics in substrate-binding domains influences transport in the ABC importer GlnPQ". In: *Nature Structural & Molecular Biology* 22.1 (Jan. 2015), pp. 57–64. ISSN: 1545-9993. DOI: 10.1038/nsmb.2929. URL: http://www.nature.com/articles/nsmb.2929.

[16] Florence Husada et al. "Conformational dynamics of the <scp>ABC</scp> transporter McjD seen by single-molecule <scp>FRET</scp>". In: *The EMBO Journal* 37.21 (Nov. 2018), pp. 1–13. ISSN: 0261-4189. DOI: 10.15252/embj.2018100056. URL: https://onlinelibrary.wiley.com/doi/10.15252/embj.2018100056.

[17] Marijn de Boer et al. "Conformational and dynamic plasticity in substrate-binding proteins underlies selective transport in ABC importers". In: *eLIFE* 8 (2019), e44652. DOI: 10.7554/eLife.44652.

[18] Nicholas J. Anthis and G. Marius Clore. "Visualizing transient dark states by NMR spectroscopy". In: *Quarterly Reviews of Biophysics* 48.1 (Feb. 2015), pp. 35–116. ISSN: 0033-5835. DOI: 10.1017/S0033583514000122. URL: https://www.cambridge.org/core/product/identifier/S0033583514000122/type/journal_article.

[19] G. Marius Clore and Junji Iwahara. "Theory, Practice, and Applications of Paramagnetic Relaxation Enhancement for the Characterization of Transient Low-Population States of Biological Macromolecules and Their Complexes". In: *Chemical Reviews* 109.9 (Sept. 2009), pp. 4108–4139. ISSN: 0009-2665. DOI: 10.1021/cr900033p. URL: https://pubs.acs.org/doi/10.1021/cr900033p.

[20] Arthur G. Palmer. "NMR Characterization of the Dynamics of Biomacromolecules". In: *Chemical Reviews* 104.8 (Aug. 2004), pp. 3623–3640. ISSN: 0009-2665. DOI: 10.1021/cr030413t. URL: https://pubs.acs.org/doi/10.1021/cr030413t.

[21] Enrico Ravera et al. "Insights into Domain–Domain Motions in Proteins and RNA from Solution NMR". In: *Accounts of Chemical Research* 47.10 (Oct. 2014), pp. 3118–3126. ISSN: 0001-4842. DOI: 10.1021/ar5002318. URL: https://pubs.acs.org/doi/10.1021/ar5002318.

[22] Qian Peter Su and Lining Arnold Ju. "Biophysical nanotools for single-molecule dynamics". In: *Biophysical Reviews* 10.5 (Oct. 2018), pp. 1349–1357. ISSN: 1867-2450. DOI: 10.1007/s12551-018-0447-y. URL: http://link.springer.com/10.1007/s12551-018-0447-y.

[23] Krutika Bavishi and Nikos Hatzakis. "Shedding Light on Protein Folding, Structural and Functional Dynamics by Single Molecule Studies". In: *Molecules* 19.12 (Nov. 2014), pp. 19407–19434. ISSN: 1420-3049. DOI: 10.3390/molecules191219407. URL: http://www.mdpi.com/1420-3049/19/12/19407.

[24] Exequiel Medina, Danielle R. Latham, and Hugo Sanabria. "Unraveling protein's structural dynamics: from configurational dynamics to ensemble switching guides functional mesoscale assemblies". In: *Current Opinion in Structural Biology* 66 (2021), pp. 129–138. ISSN: 1879033X. DOI: 10.1016/j.sbi.2020.10.016. URL: https://doi.org/10.1016/j.sbi.2020.10.016.

[25] Soumit S. Mandal. "Force Spectroscopy on Single Molecules of Life". In: *ACS Omega* 5.20 (May 2020), pp. 11271–11278. ISSN: 2470-1343. DOI: 10.1021/acsomega.0c00814. URL: https://pubs.acs.org/doi/10.1021/acsomega.0c00814.

[26] Mykola Dimura et al. "Quantitative FRET studies and integrative modeling unravel the structure and dynamics of biomolecular systems". In: *Current Opinion in Structural Biology* 40 (Oct. 2016), pp. 163–185. ISSN: 0959440X. DOI: 10.1016/j.sbi.2016.11.012. URL: http://dx.doi.org/10.1016/j.sbi.2016.11.012%20https://linkinghub.elsevier.com/retrieve/pii/S0959440X1630197X.

[27] Taekjip Ha et al. "Probing the interaction between two single molecules: fluorescence resonance energy transfer between a single donor and a single acceptor". In: *Proceedings of the National Academy of Sciences of the United States of America* 93.13 (1996), pp. 6264–6268. ISSN: 0027-8424. DOI: 10.1073/pnas.93.13.6264.

[28] Th. Förster. "Zwischenmolekulare Energiewanderung und Fluoreszenz". In: *Annalen der Physik* 437.1-2 (1948), pp. 55–75. ISSN: 15213889. DOI: 10.1002/andp.19484370105.

[29] Th. Förster. "10th Spiers Memorial Lecture. Transfer mechanisms of electronic excitation". In: *Discussions of the Faraday Society* 27.10 (1959), p. 7. ISSN: 0366-9033. DOI: 10.1039/df9592700007. URL: http://xlink.rsc.org/?DOI=df9592700007.

[30] L Stryer and R P Haugland. "Energy transfer: a spectroscopic ruler." In: *Proceedings of the National Academy of Sciences of the United States of America* 58.2 (1967), pp. 719–726. ISSN: 0066-4154. eprint: arXiv:1011.1669v3.

[31] Maxime Dahan et al. "Ratiometric measurement and identification of single diffusing molecules". In: *Chemical Physics* 247.1 (1999), pp. 85–106. ISSN: 03010104. DOI: 10.1016/S0301-0104(99)00132-9.

[32] Ashok A. Deniz et al. "Single-pair fluorescence resonance energy transfer on freely diffusing molecules: Observation of Forster distance dependence and subpopulations". In: *Proceedings of the National Academy of Sciences* 96.7 (Mar. 1999), pp. 3670–3675. ISSN: 0027-8424. DOI: 10.1073/pnas.96.7.3670. URL: http://www.pnas.org/cgi/doi/10.1073/pnas.96.7.3670.

[33] Nam Ki Lee et al. "Accurate FRET measurements within single diffusing biomolecules using alternating-laser excitation". In: *Biophysical Journal* 88.4 (2005), pp. 2939–2953. ISSN: 00063495. DOI: 10.1529/biophysj.104.054114. URL: http://dx.doi.org/10.1529/biophysj.104.054114.

[34] P. J. Rothwell et al. "Multiparameter single-molecule fluorescence spectroscopy reveals heterogeneity of HIV-1 reverse transcriptase:primer/template complexes". In: *Proceedings of the National Academy of Sciences* 100.4 (Feb. 2003), pp. 1655–1660. ISSN: 0027-8424. DOI: 10.1073/pnas.0434003100. URL: http://www.pnas.org/cgi/doi/10.1073/pnas.0434003100.

[35] Matthew Aviram et al. "Separating Structural Heterogeneities from Stochastic Variations in Fluorescence Resonance Energy Transfer Distributions via Photon Distribution Analysis". In: *The Journal of Physical Chemistry B* 110 (13 2006), pp. 6970–6978. DOI: 10.1021/jp057257.

[36] Eyal Nir et al. "Shot-Noise Limited Single-Molecule FRET Histograms: Comparison between Theory and Experiments". In: *The Journal of Physical Chemistry B* 110 (44 2006), pp. 22103–22124. DOI: 10.1021/jp063483n.

[37] Stanislav Kalinin et al. "Probability Distribution Analysis of Single-Molecule Fluorescence Anisotropy and Resonance Energy Transfer". In: *The Journal of Physical Chemistry B* 111 (34 2007), pp. 10253–10262. DOI: 10.1021/jp072293p.

[38] Stanislav Kalinin et al. "Characterizing Multiple Molecular States in Single-Molecule Multiparameter Fluorescence Detection by Probability Distribution Analysis". In: *The Journal of Physical Chemistry B* 112 (28 2008), pp. 8361–8374. DOI: 10.1021/jp711942q.

[39] Stanislav Kalinin et al. "Detection of Structural Dynamics by FRET: A Photon Distribution and Fluorescence Lifetime Analysis of Systems with Multiple States". In: *The Journal of Physical Chemistry B* 114 (23 2010), pp. 7983–7995. DOI: 10.1021/jp102156t.

[40] Yusdi Santoso, Joseph P. Torella, and Achillefs N. Kapanidis. "Characterizing single-molecule FRET dynamics with probability distribution analysis". In: *ChemPhysChem* 11 (10 2010), pp. 2209–2219. DOI: 10.1002/cphc.201000129.

[41] Joseph P. Torella et al. "Identifying molecular dynamics in single-molecule fret experiments with burst variance analysis". In: *Biophysical Journal* 100.6 (2011), pp. 1568–1577. ISSN: 15420086. DOI: 10.1016/j.bpj.2011.01.066. URL: http://dx.doi.org/10.1016/j.bpj.2011.01.066.

[42] Toma E. Tomov et al. "Disentangling subpopulations in single-molecule FRET and ALEX experiments with photon distribution analysis". In: *Biophysical Journal* 102.5 (2012), pp. 1163–1173. ISSN: 00063495. DOI: 10.1016/j.bpj.2011.11.4025. URL: http://dx.doi.org/10.1016/j.bpj.2011.11.4025.

[43] Evangelos Sisamakis et al. "Accurate Single-Molecule FRET Studies Using Multiparameter Fluorescence Detection". In: *Methods in Enzymology.* 1st ed. Vol. 475. Elsevier Inc., 2010, pp. 455–514. DOI: 10.1016/S0076-6879(10)75018-7. URL: http://dx.doi.org/10.1016/S0076-6879(10)75018-7%20https://linkinghub.elsevier.com/retrieve/pii/S0076687910750187.

[44] Anders Barth et al. "Unraveling multi-state molecular dynamics in single-molecule FRET experiments- Part I: Theory of FRET-Lines". In: (July 2021). arXiv: 2107.14770. URL: http://arxiv.org/abs/2107.14770.

[45] Douglas Magde, Elliot Elson, and WW Webb. "Thermodynamic Fluctuations in a Reacting System—Measurement by Fluorescence Correlation Spectroscopy". In: *Physical Review Letters* 29 (1972), p. 705. DOI: 10.1103/PhysRevLett.29.705.

[46] R. Rigler et al. "Fluorescence correlation spectroscopy with high count rate and low background: analysis of translational diffusion". In: *Accounts of Chemical Research* 22.10 (3 Oct. 1993), pp. 169–175. DOI: 10.1007/BF00185777.

[47] Jerker Widengren et al. "Two New Concepts to Measure Fluorescence Resonance Energy Transfer via Fluorescence Correlation Spectroscopy: Theory and Experimental Realizations". In: *The Journal of Physical Chemistry A* 105 (28 2001), pp. 6851–6866. DOI: 10.1021/jp010301a.

[48] Tedman Torres and Marcia Levitus. "Measuring Conformational Dynamics: A New FCS-FRET Approach". In: *The Journal of Physical Chemistry B* 111 (25 2007), pp. 7392–7400. DOI: 10.1021/jp070659s.

[49] Kaushik Gurunathan and Marcia Levitus. "FRET Fluctuation Spectroscopy of Diffusing Biopolymers: Contributions of Conformational Dynamics and Translational Diffusion". In: *The Journal of Physical Chemistry B* 114 (2 2010), pp. 980–986. DOI: 10.1021/jp907390n.

[50] Malte Köllner and Jürgen Wolfrum. "How many photons are necessary for fluorescence-lifetime measurements?" In: *Chemical Physics Letters* 200 (1-2 1992), pp. 199–204. DOI: 10.1016/0009-2614(92)87068-Z.

[51] C. Zander et al. "Detection and characterization of single molecules in aqueous solution". In: *Applied Physics B* 63 (1996), pp. 517–523. DOI: 10.1007/BF01828950.

[52] Michael Maus et al. "An Experimental Comparison of the Maximum Likelihood Estimation and Nonlinear Least-Squares Fluorescence Lifetime Analysis of Single Molecules". In: *Analytical Chemistry* 73 (9 2001), pp. 2078–2086. DOI: 10.1021/ac000877g.

[53] Daniel Nettels et al. "Ultrafast Dynamics of Protein Collapse from Single-Molecule Photon Statistics". In: *Proceedings of the National Academy of Sciences of the United States of America* 104 (8 2007), pp. 2655–2660. DOI: 10.1073/pnas.0611093104.

[54] Hoi Sung Chung et al. "Single-Molecule Fluorescence Experiments Determine Protein Folding Transition Path Times". In: *Science* 335 (6071 2012), pp. 981–984. DOI: 10.1126/science.1215768.

[55] Bettina G. Keller et al. "Complex RNA Folding Kinetics Revealed by Single-Molecule FRET and Hidden Markov Models". In: *The Journal of American Chemical Society* 136 (12 2014), pp. 4534–4543. DOI: 10.1021/ja4098719.

[56] Menahem Pirchi et al. "Photon-by-Photon Hidden Markov Model Analysis for Microsecond Single-Molecule FRET Kinetics". In: *Journal of Physical Chemistry B* 120.51 (2016), pp. 13065–13075. ISSN: 15205207. DOI: 10.1021/acs.jpcb.6b10726.

[57] Irina V. Gopich and Attila Szabo. "Theory of the energy transfer efficiency and fluorescence lifetime distribution in single-molecule FRET". In: *Proceedings of the National Academy of Sciences of the United States of America* 109 (20 2012), pp. 7747–7752. DOI: 10.1073/pnas.1205120109.

[58] Antonino Ingargiola, Shimon Weiss, and Eitan Lerner. "Monte Carlo Diffusion-Enhanced Photon Inference: Distance Distributions and Conformational Dynamics in Single-Molecule FRET". In: *The Journal of Physical Chemistry B* 122 (49 2018), pp. 11598–11615. DOI: 10.1021/acs.jpcb.8b07608.

[59] Irina V. Gopich and Attila Szabo. "Decoding the pattern of photon colors in single-molecule FRET". In: *Journal of Physical Chemistry B* 113.31 (2009), pp. 10965–10973. ISSN: 15206106. DOI: 10.1021/jp903671p. arXiv: NIHMS150003.

[60] Barbara K. Müller et al. "Pulsed interleaved excitation". In: *Biophysical Journal* 89.5 (2005), pp. 3508–3522. ISSN: 00063495. DOI: 10.1529/biophysj.105.064766.

[61] Ted A. Laurence et al. "Probing structural heterogeneities and fluctuations of nucleic acids and denatured proteins". In: *Proceedings of the National Academy of Sciences* 102.48 (Nov. 2005), pp. 17348–17353. DOI: 10.1073/pnas.0508584102. URL: http://www.pnas.org/cgi/doi/10.1073/pnas.0508584102.

[62] Sungchul Hohng, Chirlmin Joo, and Taekjip Ha. "Single-Molecule Three-Color FRET". In: *Biophysical Journal* 87.2 (Aug. 2004), pp. 1328–1337. ISSN: 00063495. DOI: 10.1529/biophysj.104.043935. URL: https://linkinghub.elsevier.com/retrieve/pii/S0006349504736127.

[63] Jean-Pierre Clamme and Ashok A. Deniz. "Three-Color Single-Molecule Fluorescence Resonance Energy Transfer". In: *ChemPhysChem* 6 (1 2005), pp. 74–77. DOI: 10.1002/cphc.200400261.

[64] Nam Ki Lee, Hye Ran Koh, and Seong Keun Kim. "Folding of 8-17 Deoxyribozyme Studied by Three-Color Alternating-Laser Excitation of Single Molecules". In: *Journal of the American Chemical Society* 129 (50 2007), pp. 15526–15534. DOI: 10.1021/ja0725145.

[65] Nam Ki Lee et al. "Three-Color Alternating-Laser Excitation of Single Molecules: Monitoring Multiple Interactions and Distances". In: *Biophysical Journal* 92 (1 2007), pp. 303–312. DOI: 10.1529/biophysj.106.093211.

[66] Sanghwa Lee, Jinwoo Lee, and Sungchul Hohng. "Single-Molecule Three-Color FRET with Both Negligible Spectral Overlap and Long Observation Time". In: *PLoS One* 5 (2010), e12270. DOI: 10.1371/journal.pone.0012270.

[67] Ingo H. Stein, Christian Steinhauser, and Philip Tinnefeld. "Single-Molecule Four-Color FRET Visualizes Energy-Transfer Paths on DNA Origami". In: *Journal of the American Chemical Society* 133 (12 2011), pp. 719–726.

[68] Seok W. Yim et al. "Four-Color Alternating-Laser Excitation Single-Molecule Fluorescence Spectroscopy for Next-Generation Biodetection Assays". In: *Clinical Chemistry* 58 (4 2012), pp. 707–716. DOI: 10.1373/clinchem.2011.176958.

[69] C. Ratzke, B. Hellenkamp, and Thorsten Hugel. "Four-colour FRET reveals directionality in the Hsp90 multicomponent machinery". In: *Nature Communications* 5 (2014), p. 4192. DOI: 10.1038/ncomms5192.

[70] Roman Tsukanov et al. "Conformational Dynamics of DNA Hairpins at Millisecond Resolution Obtained from Analysis of Single-Molecule FRET Histograms". In: *The Journal of Physical Chemistry B* 117.50 (Dec. 2013), pp. 16105–16109. ISSN: 1520-6106. DOI: 10.1021/jp411280n. URL: https://pubs.acs.org/doi/10.1021/jp411280n.

[71] Martin F. Peter et al. "Studying Conformational Changes of the Yersinia Type-III-Secretion Effector YopO in Solution by Integrative Structural Biology". In: *Structure* 27 (2019), 1416–1426.e3. ISSN: 18784186. DOI: 10.1016/j.str.2019.06.007. URL: https://doi.org/10.1016/j.str.2019.06.007.

[72] Paul David Harris et al. *Multi-parameter photon-byphoton hidden Markov modeling dataset*. Zenodo, Apr. 2021. DOI: 10.5281/zenodo.5566809. URL: https://doi.org/10.5281/zenodo.5566809.

[73] Paul D. Harris, Samir M. Hamdan, and Satoshi Habuchi. "Relative Contributions of Base Stacking and Electrostatic Repulsion on DNA Nicks and Gaps". In: *The Journal of Physical Chemistry B* 124 (47 2020), pp. 10663–10672. DOI: 10.1021/acs.jpcb.0c06941.

[74] C. Biernacki, G. Celeux, and G. Govaert. "Assessing a mixture model for clustering with the integrated completed likelihood". In: *IEEE Transactions on Pattern Analysis and Machine Intelligence* 22.7 (July 2000), pp. 719–725. ISSN: 01628828. DOI: 10.1109/34.865189. URL: http://journals.sagepub.com/doi/10.1177/003591577406700922%20http://ieeexplore.ieee.org/document/865189/.

[75] Gilles Celeux and Jean-Baptiste Durand. "Selecting hidden Markov model state number with cross-validated likelihood". In: *Computational Statistics* 23.4 (Oct. 2008), pp. 541–564. ISSN: 0943-4062. DOI: 10.1007/s00180-007-0097-1. URL: http://link.springer.com/10.1007/s00180-007-0097-1.

[76] Paul David Harris. *H2MMpythonlib: Simulated Models*. Version v2.0.3. Sept. 29, 2021. DOI: 10.5281/zenodo.5535302. URL: https://zenodo.org/record/5535302.

[77] Rebecca Mächtel et al. "An integrated transport mechanism of the maltose ABC importer". In: *Research in Microbiology* 170.8 (Nov. 2019), pp. 321–337. ISSN: 09232508. DOI: 10.1016/j.resmic.2019.09.004. URL: https://linkinghub.elsevier.com/retrieve/pii/S0923250819300981.

[78] "A single-molecule dissection of ligand binding to a protein with intrinsic dynamics." In: *Nature chemical biology* 9.5 (2013), pp. 313–8. ISSN: 1552-4469. DOI: 10.1038/nchembio.1213. URL: http://www.ncbi.nlm.nih.gov/pubmed/23502425.

[79] Antonino Ingargiola. "Applying Corrections in Single-Molecule FRET". In: *bioRxiv* (2017), p. 083287. DOI: 10.1101/083287. URL: https://www.biorxiv.org/content/early/2017/02/01/083287.

[80] Paul David Harris. *FRETBursts development version*. Version 0.7+29.gc9efe1a.dirty. Sept. 2, 2021. URL: https://github.com/harripd/FRETBursts/tree/polarization.

[81] Paul David Harris. *H2MM Tutorial*. Zenodo, Oct. 2021. DOI: 10.5281/zenodo.5566886. URL: https://doi.org/10.5281/zenodo.5566886.

[82] Martin F Peter et al. "Cross-validation of distance measurements in proteins by PELDOR/DEER and single-molecule FRET". In: *bioRxiv* Area 10 (2020), p. 2020.11.23.394080. DOI: 10.1101/2020.11.23.394080. URL: http://biorxiv.org/content/early/2020/11/23/2020.11.23.394080.abstract.

[83] Antonino Ingargiola et al. "Photon-HDF5". In: *Biophysical Journal* 110 (2016), pp. 25–33. ISSN: 00063495.

[84] Christian Gebhardt et al. "Molecular and Spectroscopic Characterization of Green and Red Cyanine Fluorophores from the Alexa Fluor and AF Series**". In: *ChemPhysChem* 22.15 (Aug. 2021), pp. 1566–1583. ISSN: 1439-4235. DOI: 10.1002/cphc.202000935. URL: https://onlinelibrary.wiley.com/doi/10.1002/cphc.202000935.

[85] Antonino Ingargiola et al. "FRETBursts: An open source toolkit for analysis of freely-diffusing Single-molecule FRET". In: *PLoS ONE* 11.8 (2016), pp. 1–27. ISSN: 19326203. DOI: 10.1371/journal.pone.0160716.

[86] Antonino Ingargiola. "FOpenSMFS/PyBroMo: Version 0.8.1". In: *zenodo.org* (2019). DOI: 10.5281/zenodo.3256149.

[87] Dolev Hagai and Eitan Lerner. "Systematic assessment of burst impurity in confocal-based single-molecule fluorescence detection using Brownian motion simulations". In: *Molecules* 24.14 (2019). ISSN: 14203049. DOI: 10.3390/molecules24142557.